Total reaction and $2n$-removal cross sections of 20–60A MeV ^{4,6,8}He, $^{6-9,11}$Li, and ^{10}Be on Si

R. E. Warner,[1,2,*] R. A. Patty,[2] P. M. Voyles,[2] A. Nadasen,[3] F. D. Becchetti,[4] J. A. Brown,[1] H. Esbensen,[5] A. Galonsky,[1] J. J. Kolata,[6] J. Kruse,[1] M. Y. Lee,[4] R. M. Ronningen,[1] P. Schwandt,[7] J. von Schwarzenberg,[6] B. M. Sherrill,[1] K. Subotic,[8] J. Wang,[1] and P. Zecher[1]

[1]*National Superconducting Cyclotron Laboratory, East Lansing, Michigan 48824*
[2]*Oberlin College, Oberlin, Ohio 44074*
[3]*University of Michigan, Dearborn, Michigan 48128*
[4]*University of Michigan, Ann Arbor, Michigan 48109*
[5]*Argonne National Laboratory, Argonne, Illinois 60439*
[6]*University of Notre Dame, Notre Dame, Indiana 46556*
[7]*Indiana University Cyclotron Facility, Bloomington, Indiana 47405*
[8]*Institute of Nuclear Sciences, VINCA, Belgrade 11001, Yugoslavia*

(Received 1 March 1996)

Total reaction cross sections, σ_R, of 20–60A MeV ^{4,6,8}He, $^{6-9,11}$Li, and ^{10}Be were measured by injecting magnetically separated, focused, monoenergetic, identified secondary beams of those projectiles into a Si detector telescope and measuring their energy-deposition spectra. These σ_R's, accurate to about 3%, were compared with predictions of optical, strong absorption, and microscopic models. The latter gave the best overall fit to the data, providing long-tailed matter densities were assumed. The best available optical potentials generally overpredicted the data by about 10%. Strong absorption calculations, in which the isospin-dependent term is quite important, were often unsuccessful, especially for projectiles with large neutron excess. Two-neutron removal cross sections were measured for ^{6}He and ^{11}Li; the ^{11}Li data were slightly overpredicted by a microscopic model which includes correlation effects for the ^{11}Li valence neutrons. Both $2n$ and $4n$ removal from ^{8}He were observed, in about a 2:1 ratio. Subtraction analysis of the data indicates that ^{4}He is a good core within ^{6}He and ^{8}He, as is ^{9}Li within ^{11}Li. [S0556-2813(96)01810-9]

PACS number(s): 25.60.Dz, 25.70.Mn, 24.10.−i, 27.20.+n

I. INTRODUCTION

The total nuclear reaction cross sections (σ_R) of stable nuclei have long been of interest since they tell us about the radii and transparency of these nuclei and give clues to their structure. Often this information is supplementary to that obtained through other measurements. For instance, accurate elastic-scattering measurements can determine the optical-model potential parameters for a system, which in turn allow σ_R to be deduced. On the other hand, measured σ_R values can serve as important constraints in phenomenological optical-model analyses [1].

Measurements of σ_R, however, assume new importance with the development of radioactive nuclear beams (RNB's). The low intensities and poor collimation of such beams often preclude the large variety of sophisticated and detailed measurements available with stable beams: elastic scattering with sharp angular resolution, inelastic scattering to well-resolved excited states, studies of specific reactions, etc. Thus, at present, σ_R is one of the few measurable parameters of an unstable nucleus.

The first data for unstable nuclei [2] were high-energy measurements (800A MeV) of the interaction cross section σ_I, which includes only those reactions which destroy the projectile, but excludes target reactions which leave the projectile intact. These mainly determined interaction radii and, in particular, revealed the existence of neutron-halo nuclei [3] such as ^{6}He, ^{11}Li, and ^{11}Be.

Low-energy σ_R measurements now seem to be a necessary complement to the high-energy σ_I data, since the increase of the nucleon-nucleon interaction cross section at low energies makes σ_R more sensitive to the nuclear matter distribution in the tail region of the nucleus [4]. For instance, reaction cross sections of the proton-halo candidate ^{8}B show enhancement at $\sim$40A MeV [4] though not at higher energies [2]. Nuclear and Coulomb effects [5] also are more easily separated at low energies.

Throughout these energy ranges ($\sim$20–800A MeV) there are too few data, measured at different energies and on different targets, for the systematics of σ_R to be well established. Special, high-efficiency methods for measuring σ_R's of unstable nuclei are required by the low available RNB fluxes. These include the $4\pi-\gamma$ method [6], absorbers placed in counter telescopes [7], and the use of Si and CsI detectors as active targets [4,8]. There appear to be normalization problems in comparing measurements by different methods. Therefore, to improve this data base, we have measured σ_R for all bound He and Li nuclei (except ^{3}He) on ^{nat}Si, using a multidetector Si telescope. To complete the systematics, ^{10}Be measurements were included since ^{10}He and ^{10}Li are unbound. The projectiles thus include both stable and radioactive nuclei, and normal and halo nuclei. For each projectile, measurements were made at several energies between 20 and 60A MeV; thus our data provide tests for several reaction theories, which predict substantial energy dependence in this energy range. We also compare our measurements with all other available data below 100A MeV.

*Permanent address: Oberlin College, Oberlin, OH 44074.

For the two-neutron-halo nuclei, $2n$ removal is one of the strongest reaction channels [5,7,9]. Both the magnitude and energy dependence of σ_{-2n} are likely to give us information about the halo. In Sec. III C, we report measurements of σ_{-2n} for ^{6}He and ^{11}Li, and of $(\sigma_{-2n}+\sigma_{-4n})$ for ^{8}He, and compare them with similar reported data. These three nuclei make an interesting set since their $2n$-separation energies range from 0.3 MeV (^{11}Li) to 2.1 MeV (^{8}He). We show also that our method straightforwardly determines the normalization of σ_{-2n} relative to σ_R.

The microscopic (Glauber) theories [10–12] provide an appealing physical picture in which reaction cross sections result from individual nucleon-nucleon collisions in projectile and target. We show that they adequately describe our σ_R results, as well as σ_{-2n} for ^{11}Li, and are generally superior to the optical and strong absorption models in fitting the data.

Section II of this paper describes our experimental procedure. Section III describes the data analysis procedure and the results obtained; Sec. IV discusses these results and compares them with the predictions of optical, strong absorption, and microscopic models. A brief summary and our conclusions are presented in Sec. V.

II. EXPERIMENTAL PROCEDURE

Our method of measuring σ_R requires injecting a focused, monoenergetic, identified beam of the projectile of interest (selected by magnetic analysis and position-sensitive detectors) into a stack of Si detectors [4,8]. Each projectile's energy deposition in each detector is measured to determine in which detector, if any, it undergoes a nuclear reaction.

The projectiles were produced at the National Superconducting Cyclotron Laboratory by a primary 80A MeV beam of ^{18}O, up to 50 pnA in intensity, bombarding an 0.8 or 1.2 g/cm^2 Be target. The secondary beams were then transmitted through the A1200 analyzing system [13]; their energy dispersion was minimized with CH_2 wedges [14]. Slits were used which gave momentum resolution 0.5% (FWHM); consequently, the energy resolution for particles losing energy only through ionization was usually close to 1% FWHM. Injection energies ranged from 55A MeV for ^{8}He to 68A MeV for ^{10}Be, and were usually chosen so that projectiles stopped near the middle of a detector.

Figure 1 (not to scale) shows our detector stack. All detectors but the first position-sensitive detector (PSD) were close packed with $\sim$1 cm center-to-center separation.

The PSD's and ΔE detector had thicknesses 200 μm and 1 mm, respectively. Each Si(Li) counter (Li-drifted Si) was 5 mm thick, and was tested for energy resolution and full depletion by α particles from a radioactive source, incident from both its front and back face. The first three Si(Li)'s had 23.9 mm diameter, and the final three had 43.0 mm diameter to minimize event misidentification due to imperfect beam alignment or outscattering from the first few counters. ''Contaminants'' present in the detectors cause negligible systematic errors when all reactions are attributed to ^{28}Si, since model calculations [15] predict σ_R's which differ by less than 0.5% for ^{28}Si and $^{\rm nat}$Si, and the Li content is $\leqslant$0.01% throughout the detectors.

Fast mean-timed signals from the ΔE and first Si(Li) detectors provided the trigger for recording events on magnetic tape. During data acquisition, pileup signals were recorded from the ΔE and first two Si(Li) detectors, but were not used to reject events. During analysis, pileup was found to be negligible at the data rates we employed, which were typically 200–400/s.

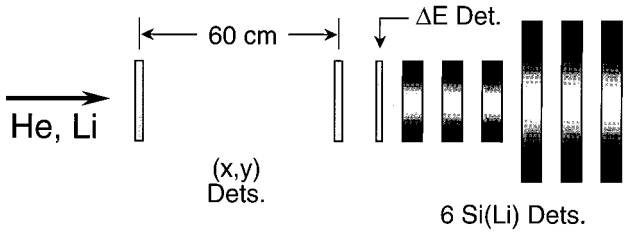

FIG. 1. Silicon detector stack (not to scale) used in this experiment.

III. DATA ANALYSIS AND RESULTS

A. General analysis procedure

We obtained projectile energy-deposition spectra such as those shown in Fig. 2, where counts vs total energy deposited in the telescope are shown for ^{6}Li, ^{8}He, and ^{11}Li. The off-scale peaks are produced by nonreacting projectiles, while events to the left of the vertical dashed lines near 60 MeV/nucleon were assumed to be reactions. The ^{6}Li spectrum (Fig. 2) typifies that of most projectiles studied, with the reaction events forming a featureless continuum. These continua were arbitrarily but nicely fitted, except at the lowest energies, by quadratic functions (dashed curves). However, ^{11}Li showed a prominent two-neutron-removal peak above the continuum caused by core reactions, as did ^{6}He. On average, ^{11}Li breaks up after losing half its incident energy; the two neutrons then carry off two-elevenths of the remaining kinetic energy. Thus the $2n$-removal group should peak at ten-elevenths of the energy of the nonreacting particles, as is observed in Fig. 2. Finally, the ^{8}He spectra (Fig. 2) showed structure due to both $2n$ and $4n$ removal. Analysis of the neutron-removal data will be discussed in Sec. III C.

Each detector was calibrated in energy from the known energy losses of both the projectiles of interest and beam contaminant groups. All analyzed events were required to pass tight energy gates, appropriate to the projectile of interest, for both PSD's and the ΔE counter. Projectiles also were required to pass within 6 mm of the center of the first PSD and within 4 mm of the center of the second one. It was verified that these radius gates could be increased by 50%, and the three ΔE gates similarly expanded, with negligible effect on our results.

The energy-deposition spectra shown in Fig. 2 were obtained using only the five gates (three energies, two radii) for the PSD and ΔE counters. From them we obtain a nuclear reaction probability η_1, defined [4,8] as the ratio of reactions to total events. The subscript ''1'' denotes that the reactions took place in or beyond the first Si(Li) detector.

Spectra were next obtained for projectiles known *not* to react in the first Si(Li) detector. The reaction probability η_2,

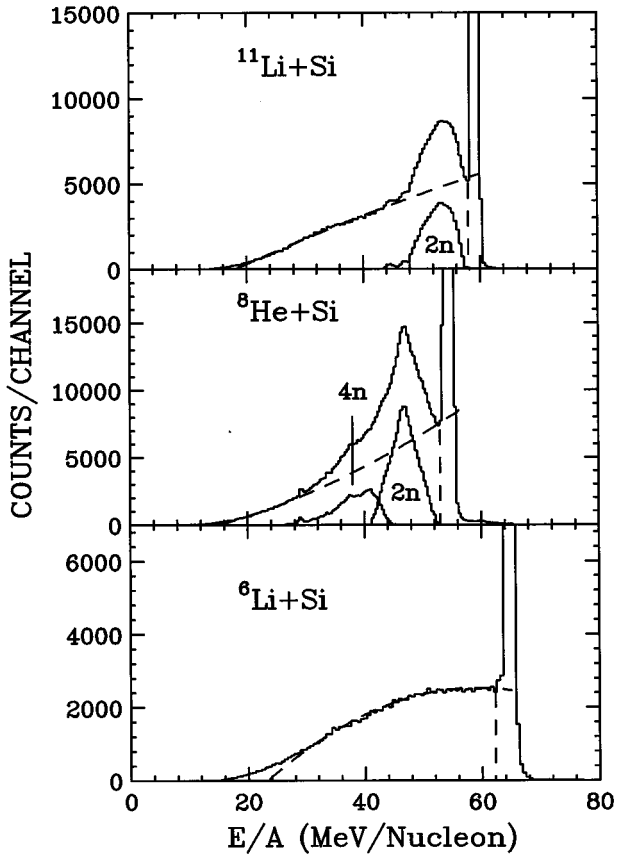

FIG. 2. Energy-deposition spectra of ^{6}Li, ^{8}He, and ^{11}Li projectiles in Si telescope, with structure due to $2n$ removal from ^{11}Li, and both $2n$ and $4n$ removal from ^{8}He, indicated. Channel widths are approximately 0.4 MeV/nucleon. Dashed vertical lines near 60 MeV/nucleon show division between reacting and nonreacting projectiles.

for reactions occurring in counter 2 or beyond, was found from spectra taken with an additional ΔE_1 energy gate [the subscript to ΔE denotes Si(Li) detector 1] which excludes particles reacting in detector 1. The difference between η_1 and η_2 determines the likelihood for reactions to occur in detector 1, and thus σ_R for the interval between the energies at which nonreacting particles enter and leave that detector. Finally, the reaction probability η_n was found for each active counter by gating on energy losses in all preceding counters.

Two corrections were then made to the raw η_n's. (1) Some low-Q events fall under the off-scale peaks shown in Fig. 2, and are therefore wrongly counted as stopping, not reacting, projectiles; reaction yields were therefore extrapolated to the center of the peaks. Whether linear or quadratic fits to the counts in nearby reaction channels were tried, the differences $(\eta_n - \eta_{n+1})$ were generally small enough to determine σ_R to $\pm 2\%$. (2) Some projectiles react just before leaving the nth counter. Thus their signals satisfy the ΔE_n gate and they are wrongly counted as reacting in the $(n+1)$st counter. By analyzing with different gate widths ΔE_n and extrapolating to zero gate width, we concluded that this effect also contributes no more than $\pm 2\%$ uncertainty to σ_R. Thus we deduce a $\pm 3\%$ random error due to systematic effects, compared to which statistical uncertainty is negligible. Data from different runs with the same projectile also were consistent to much better than our stated error.

B. Results for σ_R

We relate σ_R to the η_n's by considering N projectiles of energy E entering a slab of thickness Δx, in which there are ρ nuclei per unit volume, and leaving it with energy $E-\Delta E$. The fraction which reacts is

$$-(dN/N)=\sigma_R(E)\rho\ dx=[\sigma_R(E)\rho\ dE]/(dE/dx). \quad (1)$$

We integrate Eq. (1) for the nth detector, which has thickness T, and which N_i particles enter and N_f leave with energies E_i and E_f, respectively, obtaining

$$\ln(N_i/N_f)=\overline{\sigma_R}\ \rho\ T, \quad (2)$$

where the energy-averaged reaction cross section $\overline{\sigma_R}$ is defined by

$$\overline{\sigma_R}T=\int_{E_f}^{E_i}[\sigma_R(E)dE]/(dE/dx). \quad (3)$$

Straightforward algebra produces

$$(N_i/N_f)=(1-\eta_{n+1})/(1-\eta_n). \quad (4)$$

Stopping powers (dE/dx) are taken from Biersack and Ziegler [16] and, by comparison with other range tables [17], are believed accurate to about 1%.

We present our σ_R data in Figs. 3–5 and in Table I and compare them with the few similar existing data. The horizontal ''error bars'' display, for each detector, the interval between incident and exit energies for a nonreacting particle. These energies, like the stopping powers, are considered accurate to 1%. The plotted uncertainties in σ_R are only those systematic errors described earlier; statistical uncertainties are negligible in comparison. The energy dependence of our ^{4}He data is consistent with measurements made at two other laboratories: one which injected a secondary beam tagged by elastic-scattering coincidences [18] into an active Si detector; and the other using the conventional transmission method [19]. However, our absolute σ_R's are higher than those of [19]. The present results for ^{8}He and ^{11}Li have higher precision, and seem lower, than others of σ_R averaged from 0 to about 25A MeV using a single active Si detector [20]. One datum for ^{9}Li+^{27}Al, actually the result of two transmission measurements [7,21] exists at 80A MeV. Since all our model calculations give less than 3% difference for Al and Si targets, we compare it with our data in Fig. 5, where it is seen to be too low to be consistent with our data.

C. Results for σ_{-2n}

Yields in the $2n$-removal peaks for both ^{11}Li and ^{6}He were obtained by fitting a quadratic function, such as that shown fitting the ^{6}Li spectrum in Fig. 2, to the yield in regions on either side of the peak. σ_{-2n} is then determined by the difference in the peak areas for consecutive counters.

Two systematic errors arise in the data analysis. (1) There is uncertainty in the fitting process, since the underlying continuum spectra change shape from one detector to the next, as the projectile loses energy. (2) ^{11}Li (for example) disso-

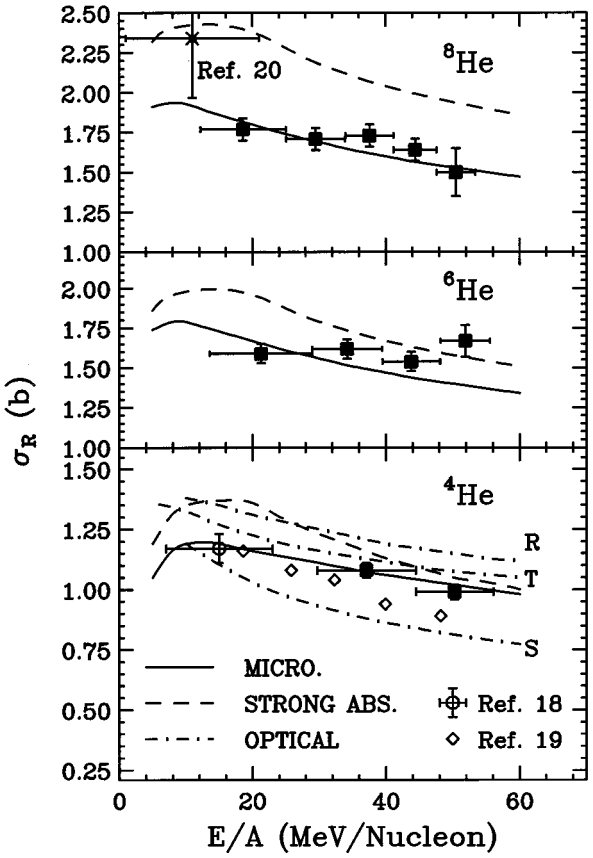

FIG. 3. Measured σ_R (solid data points) vs energy for ^{4,6,8}He in Si compared with predictions of microscopic, optical, and strong absorption models (see text) and data from three other laboratories. Horizontal ''error bars'' show energy range in which projectiles can react in each detector. R, S, and T designate optical-model predictions using Rebel, Satchler, and Tatischeff [26–28] parameters.

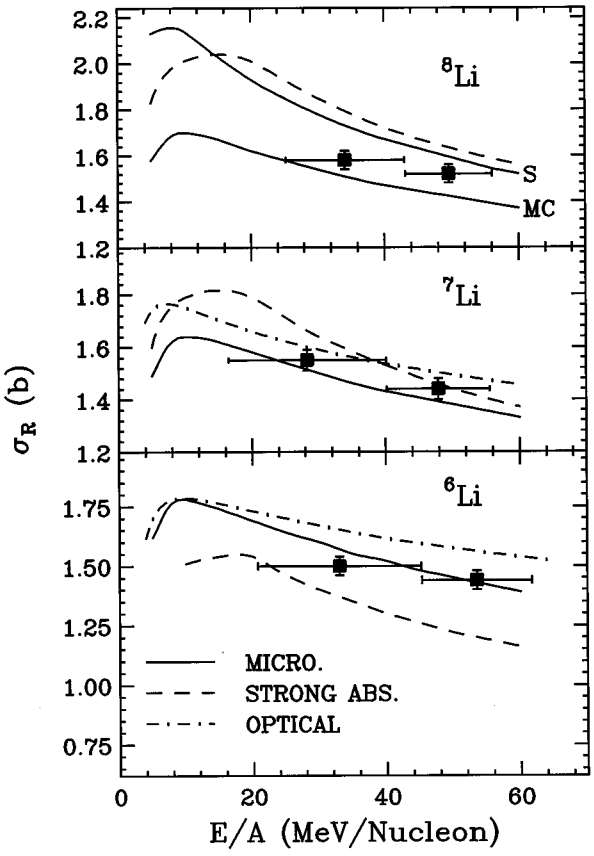

FIG. 4. Similar to Fig. 3, for $^{6-8}$Li. Two microscopic predictions for ^{8}Li use matter densities predicted by microscopic cluster (MC, [35]) and shell (S, [39]) models.

ciates into a ^{9}Li fragment which initially has about the same velocity, and therefore the same (dE/dx). Reactions occurring near the back of the nth detector may allow that detector's signal to satisfy its ΔE gate, so that the reaction is incorrectly placed in the $(n+1)$st detector. To estimate this effect, energy-loss spectra were calculated for fragments dissociating throughout the detector, using known momentum distributions for ^{6,8}He [22] and ^{11}Li [23]. The fractions of those spectra lying inside the energy gate ΔE_n determined an effective ''dead-layer'' thickness for that projectile and detector. The raw cross section for a detector was then corrected by subtracting those reactions which occurred but were not detected in the previous counter, and adding those lost in its own dead layer. This correction is relatively small for intermediate counters, since varying the assumed momentum distribution changes the entrance and exit corrections by similar amounts; for these counters, we estimate systematic errors of about $\pm 10\%$. It is more serious for the first and last counters for which, considering the uncertainty in the momentum distributions [22,23], we estimate systematic errors of $\pm 15\%$.

Our results, shown in Fig. 6 and in Table II, include σ_R averaged for the energy ranges of individual detectors (data points) and over the projectile's entire energy range (hatched horizontal bars). The latter value is quite accurate, since it is determined entirely from the first counter's spectrum (Fig. 2) rather than difference spectra; i.e., it requires no entrance or exit corrections.

We know of no other measurements of σ_{-2n} on Si for these projectiles. Later, we compare our ^{11}Li data with those available for other targets.

For ^{8}He, Fig. 6 shows the sum of σ_{-2n} and σ_{-4n} since the two peaks could not be accurately resolved in all spectra. Generally it appeared (Fig. 2) that $\sigma_{-2n}/\sigma_{-4n} \simeq 2$ as is also observed [24] at high energy for ^{8}He+C. The dominance of $2n$ over $4n$ removal is nontrivial, since shell-model calculations using the Cohen-Kurath 616-2BME interaction show that ^{8}He has only about 20% parentage from the ^{6}He ground state [25]. Production of any ^{6}He excited state is immediately followed by its $2n$ decay to ^{4}He. It therefore follows that the ^{6}He fragments are mainly sequential decay products of the unstable nucleus ^{7}He, whose ground state can decay only to $^6\mathrm{He}+n$. Production of this nucleus by single-nucleon removal should be prolific, since it has a $(3/2)^-$ ground state and $(p_{3/2})^4$ is the dominant valence neutron configuration for ^{8}He.

IV. DISCUSSION AND COMPARISON WITH THEORY

A. Optical-model predictions

Optical-model calculations of σ_R were made, using the code SNOOPY8Q, for those projectiles for which potential pa-

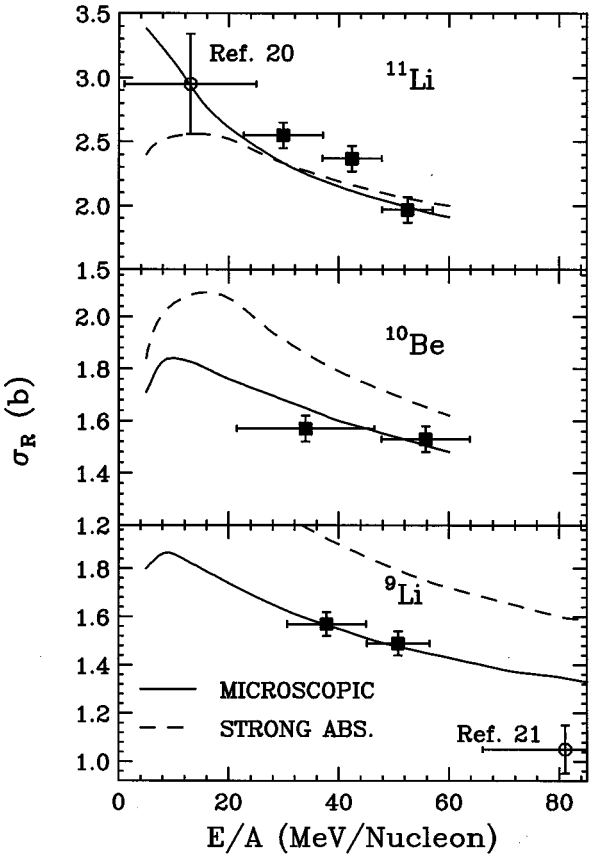

FIG. 5. Similar to Fig. 3, for ^{9,11}Li and ^{10}Be.

rameters are available for ^{28}Si targets: ^{4}He [26–28], and ^{6,7}Li [29,30]. The results are shown by dot-dashed curves in Figs. 3 and 4.

For ^{4}He, the dependence on lab energy E of the real well depths was obtained using the prescription of Nadasen and Roos [31], i.e.,

$$V = V_0 - \beta \ln E, \tag{5}$$

with β chosen to make $V=0$ at 3.5 GeV. The best ^{4}He fit (curve labeled ''T''), which overpredicted our data by only 10%, was obtained with the Tatischeff-Brissaud potentials [28] which were deduced from 41 MeV/nucleon elastic scattering data. Calculations with parameters deduced from the 7 and 26 MeV/nucleon data [26,27] failed to predict the magnitudes of our data and those of Auce *et al.* [19], but reproduce their energy dependence.

The ^{6,7}Li optical potential parameters [29,30] were found by fitting precise elastic-scattering data covering a large angular range at 35 and 50A MeV. Energy dependences of these parameters, determined during the analysis, also gave acceptable fits to low-energy elastic-scattering data. However, they overpredict our ^{6}Li and ^{7}Li results by about 10 and 5 %, respectively. We have not found a different set of optical parameters which would lower the predictions while preserving the fit to the elastic data. It appears that even optical potentials which provide good fits to elastic scattering data cannot predict reaction cross sections to better than 10%.

TABLE I. Measured σ_R for He, Li, and Be nuclei on Si, averaged between energies per nucleon E_1 and E_2.

Nucleus	E_1 (MeV/nucleon)	E_2 (MeV/nucleon)	σ_R (b)
^{4}He	29.7	44.5	1.08±0.03
^{4}He	44.5	56.1	0.99±0.03
^{6}He	13.7	29.0	1.59±0.06
^{6}He	29.0	39.5	1.62±0.06
^{6}He	39.5	48.1	1.54±0.06
^{6}He	48.1	55.6	1.67±0.10
^{8}He	12.2	25.1	1.77±0.07
^{8}He	25.1	33.9	1.71±0.07
^{8}He	33.9	41.2	1.73±0.07
^{8}He	41.2	47.6	1.64±0.07
^{8}He	47.6	53.4	1.50±0.15
^{6}Li	20.8	45.2	1.50±0.05
^{6}Li	45.2	61.8	1.44±0.05
^{7}Li	16.5	40.1	1.55±0.05
^{7}Li	40.1	55.6	1.44±0.05
^{8}Li	25.3	43.0	1.58±0.05
^{8}Li	43.0	56.2	1.52±0.05
^{9}Li	30.6	45.1	1.57±0.05
^{9}Li	45.1	56.6	1.49±0.05
^{11}Li	22.7	37.1	2.55±0.10
^{11}Li	37.1	47.9	2.37±0.10
^{11}Li	47.9	57.1	1.97±0.10
^{10}Be	21.3	46.7	1.57±0.05
^{10}Be	46.7	63.9	1.53±0.05

B. Strong-absorption models

The simplest existing models for nuclear reactions are the strong absorption models; they assume that reactions occur whenever two nuclei, traveling on Coulomb trajectories, make geometrical contact. These models differ mainly in their parametrization of the interaction radius. The most recent formulation is the model of Shen *et al.* [15], which better fits the data for many systems, at low to intermediate energies, than do earlier models. In Figs. 3–5, predictions of the Shen model (dashed curves) are compared with our nine data sets. The isospin-dependent term in this model is important for nuclei with large neutron excess. Thus, while the predictions are rather good for projectiles with $N \approx Z$, they far exceed the data for ^{8}He, ^{9}Li, and even ^{10}Be. However, they give an excellent fit for ^{11}Li. The lack of consistency in such a ''broadbrush'' model, which necessarily ignores such important details as $2n$-separation energy and pairing effects, is hardly surprising. Other calculations (not shown) were done with the Kox model [32]. For all these projectiles it gave results which were very similar to, but lower than, those of the Shen model (by no more than 10%).

C. Microscopic model

The microscopic models [10–12] attribute nucleus-nucleus reactions to the combined effects of collisions between pairs of nucleons in the target and projectile. Thus the three ingredients which enter the calculations are the

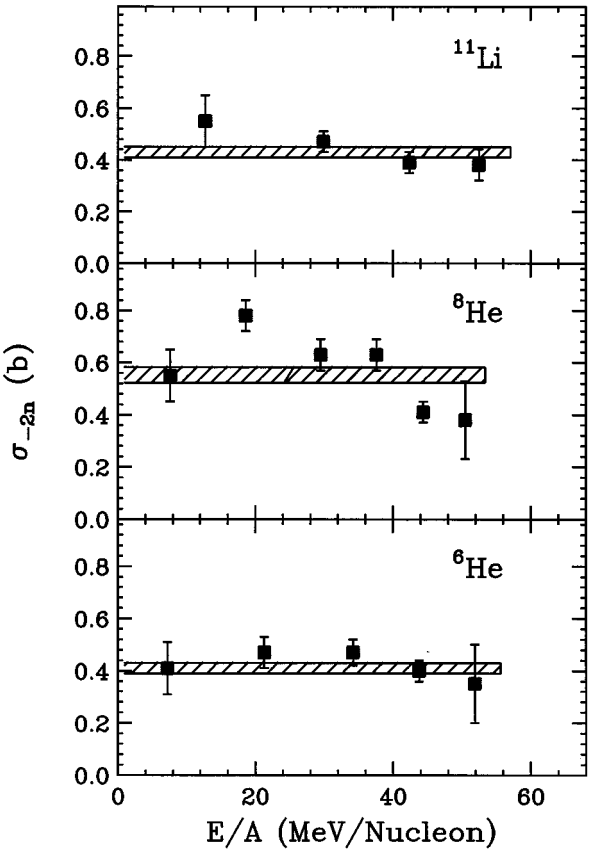

FIG. 6. Measured cross sections (solid data points) on Si for $2n$ removal from ^{6}He and ^{11}Li, and $(2n+4n)$ removal from ^{8}He. The hatched bar in each panel indicates a cross section averaged from zero to energy of incidence on our telescope; vertical thickness of bar indicates experimental uncertainty.

nucleon-nucleon total cross section and the matter densities in the colliding nuclei. We used the Charagi-Gupta [33] parametrization of σ_{NN}, and for the target density used the three-parameter-Fermi form factor for the charge density of ^{28}Si as determined by electron scattering [34]. Projectile density distributions were taken from various sources, listed in Table III.

The sensitivity of the calculations to various projectile matter distributions was explored. Long-tailed form factors are required for microscopic calculations since important contributions to σ_R come from large impact parameters [12]. Thus, single harmonic-oscillator (HO) form factors, chosen to reproduce the rms radii determined by electron scattering [34], usually gave poor results since they underestimate the matter content of the tail. For example, σ_R's of only 1.0–1.2 b were predicted for ^{6}Li and ^{7}Li with HO form factors which reproduced their rms radii. However, for ^{6,8}He Tanihata *et al.* [36] found two-term HO functions, with separate s- and p-orbital HO size parameters, which fitted the rms radii of ^{4,6,8}He deduced from high-energy σ_I measurements; further, these give $\rho(r)$'s nearly identical to those determined from the microscopic cluster model [37]. The fit they gave was quite good for ^{8}He but not ^{6}He data, whose σ_R we find to have a surprisingly weak energy dependence.

Data for three nuclei were fitted with Woods-Saxon form factors

TABLE II. Measured cross sections on Si for $2n$ removal from ^{6}He and ^{11}Li, and $(2n+4n)$ removal from ^{8}He, averaged between energies per nucleon E_1 and E_2.

Nucleus	E_1 (MeV/nucleon)	E_2	σ_{-xn} (b)
^{6}He	0.0	13.7	0.41±0.10
^{6}He	13.7	29.0	0.47±0.06
^{6}He	29.0	39.5	0.47±0.05
^{6}He	39.5	48.1	0.40±0.04
^{6}He	48.1	55.6	0.35±0.15
^{6}He	0.0	55.6	0.41±0.02
^{8}He	0.0	12.2	0.55±0.10
^{8}He	12.2	25.1	0.78±0.06
^{8}He	25.1	33.9	0.63±0.06
^{8}He	33.9	41.2	0.63±0.06
^{8}He	41.2	47.6	0.41±0.04
^{8}He	47.6	53.4	0.38±0.15
^{8}He	0.0	53.4	0.55±0.03
^{11}Li	0.0	22.7	0.55±0.10
^{11}Li	22.7	37.1	0.47±0.04
^{11}Li	37.1	47.9	0.39±0.04
^{11}Li	47.9	57.1	0.38±0.06
^{11}Li	0.0	57.1	0.43±0.02

$$\rho(r)=\rho_0/\{1+\exp[(r-R_0)/a]\} \quad (6)$$

which reproduce the rms charge radii determined in electron scattering [34]; the parameters are given in Table IV. The rms radius taken for ^{10}Be is that known for ^{10}B [34]. For nuclei other than those listed in Table IV, Woods-Saxon (WS) form factors reproducing their rms radii usually gave fits as good as those shown in Figs. 3–5. This was true, in particular, for ^{8}He, but for ^{6}He the fit was about 0.3 b lower than that shown in Fig. 3. ^{6}He is a recognized halo nucleus with $2n$-separation energy of only 0.97 MeV and $2n$-halo thickness of ~0.8 fm [25,38], and evidently the WS form factor inadequately accounts for nuclear reactions in the tail region.

D. The ^{8,9,11}Li results: General comments

Matter densities for $^{7-9}$Li based on the microscopic cluster model [35], and for ^{7,8}Li based on the shell model [39], were provided by authors of those papers. The two gave very close agreement for ^{7}Li but, as shown in Fig. 4, bracket the ^{8}Li data. ^{8}Li is of interest, among other reasons, in being the mirror nucleus of the proton halo candidate ^{8}B [4]. The

TABLE III. Matter distributions used for projectiles in microscopic calculations.

Projectile(s)	Distribution	Reference
^{4}He, ^{6}Li, ^{10}Be	Woods-Saxon	[34]
^{6,8}He	Two-term harmonic oscillator	[24]
$^{7-9}$Li	Microscopic cluster model	[35]
^{11}Li	Hartree-Fock	[36]

TABLE IV. Woods-Saxon form-factor parameters for three nuclei; all distances in fm.

Nucleus	R_0	a	$r_{\rm rms}$
^{4}He	1.5	0.308	1.63
^{6}Li	2.0	0.552	2.57
^{10}Be	2.0	0.511	2.45

shell-model densities for ^{8}Li are nearly identical to those which fitted our ^{8}B data [4], and consequently they predict the same σ_R. The microscopic cluster model finds significant differences between these mirror nuclei, predicting rms radii $r_n = 2.58$ fm for ^{8}Li and $r_p = 2.73$ fm for ^{8}B. Thus this model provides no support for a neutron halo in ^{8}Li and consequently predicts a lower σ_R, thereby better fitting our data (see Fig. 4).

^{9}Li is of some importance since three-body models of ^{11}Li must treat ^{9}Li as an inert core; nevertheless, it must have cluster structure as described by the microscopic cluster model. Matter densities from this model overpredict our data by only a small amount. We note also that the 80 MeV ^{9}Li+Al datum (Fig. 5) lies well below our model predictions.

Three contemporary models of ^{11}Li (hyperspherical harmonic, coordinate space Faddeev, and the cluster orbital shell-model approximation, or COSMA) are described in some detail in [40]. Predictions using their matter densities are compared in Fig. 7 with our data and the prediction from Fig. 5. In the energy range of our data they are similar, with the data favoring the Faddeev L5D function. The valence neutron density for the COSMA model has the steepest exponential falloff. Consequently the other models predict larger σ_R's at very low energies where, as pointed out earlier [4], σ_R has greatest sensitivity to the matter distribution in the tail. Thus experiments at these very low energies, even though technically difficult, would be quite interesting for discriminating between these models.

There appear to be no other σ_R data for ^{11}Li with Si data so, to display their systematics, we present our results (solid squares) with available σ_R (or σ_I) data for C and Pb [5,21,36,41] in Fig. 8. There they are compared with predictions of the microscopic theory of Esbensen and Bertsch [43], which has been successfully applied to the 800*A* MeV data. The data, other than for C and Pb at 43 and 75 MeV/nucleon [41], are successfully fitted by the theory.

E. 2*n* and 4*n* removal: Theory and discussion

Again, there seem be no other measurements of $2n$ removal from ^{11}Li by Si, so we compare our data (solid squares) in Fig. 9 with those available for C and Pb [5,21,42,44]. There are no C data below 80*A* MeV, so a Be datum [44] is plotted with them. These data are also compared with predictions based on the microscopic model of [43], which include contributions from both the nuclear- and Coulomb-induced breakup. We note that Coulomb dissociation plays a significant role for the Si target; at 30*A* MeV it is responsible for about 150 mb, while nuclear breakup gives 380 mb for a total of 530 mb. These data confirm the predicted energy dependence though with some large fluctuations, particularly in the C data. The Si data, with their relatively small uncertainties, lie below the predictions.

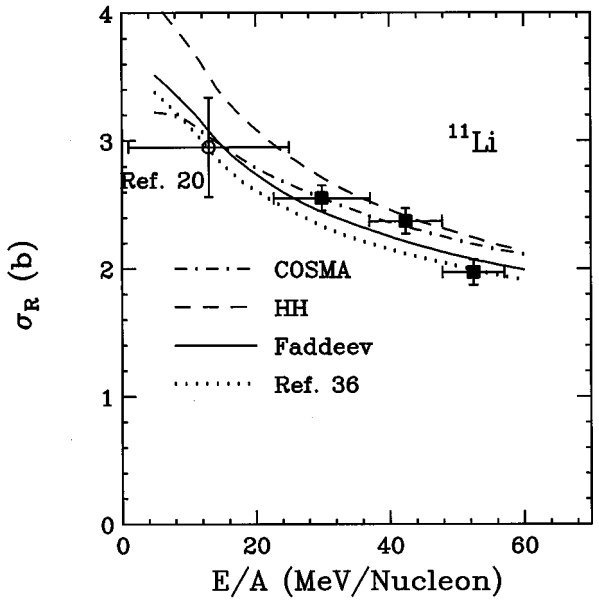

FIG. 7. ^{11}Li σ_R data compared with microscopic predictions using matter densities taken from four models [36,40].

Tanihata *et al.* [24] demonstrated that the high-energy σ_I data contain an important, intuitive relationship: e.g.,

$$\sigma_I(^6\mathrm{He}) - \sigma_{-2n}(^6\mathrm{He}) \approx \sigma_I(^4\mathrm{He}). \quad (7)$$

In other words, the nuclear reactions in which ^{6}He engages in are just those which the bare ^{4}He core would have, plus $2n$ removal. They found a similar relationship to hold for ^{4,8}He:

$$\sigma_I(^8\mathrm{He}) - \sigma_{-2n}(^8\mathrm{He}) - \sigma_{-4n}(^8\mathrm{He}) \approx \sigma_I(^4\mathrm{He}). \quad (8)$$

Thus, they deduced that ^{4}He is a good core for both ^{6}He and ^{8}He; the latter is consequential since five-body calculations for ^{8}He [45] assume an α-particle core. Further, Tanihata *et al.* find that a relationship similar to Eq. (7) fails to hold between $2n$ removal from ^{8}He and the ^{6,8}He interaction cross sections; therefore, ^{6}He is not a good core for ^{8}He.

Our measurements provide an opportunity to test these relationships—which clearly require that the intermediate nuclei (^{5,7}He, ^{10}Li) be unstable against neutron emission—at lower energies. We define $\sigma_{\rm CORE}$ to be the ''core'' cross section for events underlying the $2n$- and $4n$-removal peaks in Fig. 2. Thus, $\sigma_{\rm CORE}$ represents the ^{6}He and ^{11}Li reaction cross sections with $2n$-removal subtracted, and the ^{8}He reaction cross section with both $2n$- and $4n$-removal subtracted. (For ^{4}He, $\sigma_{\rm CORE} = \sigma_R$ by definition.) We can in fact determine $\sigma_{\rm CORE}$ with greater accuracy than σ_{-2n}, since the only systematic uncertainty arises from separating the continuum and xn-removal peaks. There are no entrance and exit corrections which, for σ_{-2n}, require redistribution of the peak events between detectors.

Our data are presented in Fig. 10. They show that, even at these lower energies, $\sigma_{\rm CORE}$ is nearly independent of projectile type. This outcome is perhaps surprising, since effects

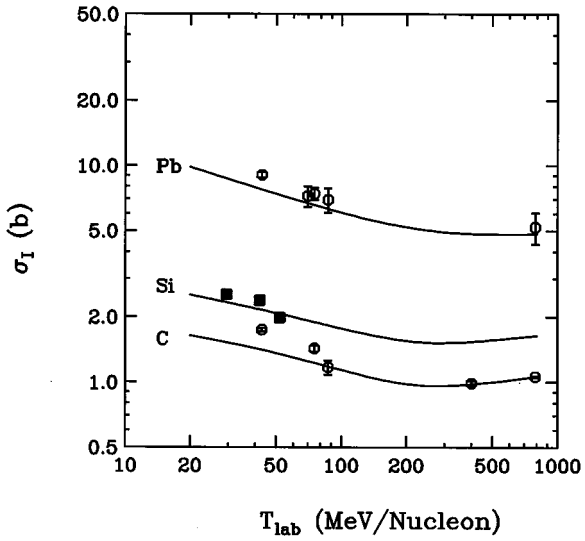

FIG. 8. Total reaction (or interaction) cross sections for ^{11}Li on C, Si, and Pb vs energy, compared with microscopic model predictions [43]. Present Si data are solid squares; open circles represent C and Pb data from [5,21,36,41].

which might prevent it may be stronger at low energy. One such effect is transfer reactions between valence neutrons and the target. Another is possible shielding of the core from the target by the valence neutrons; from the microscopic model, these interact more strongly with the target at low energy, so that a bare α particle could have a better chance of interacting with the target than one inside ^{6}He. Further, the theoretical basis of Eq. (7) was proposed [46] for high-energy data. Thus, we too find that ^{4}He is a good core for both ^{6,8}He, and also that ^{9}Li is a good core for ^{11}Li. The inequality

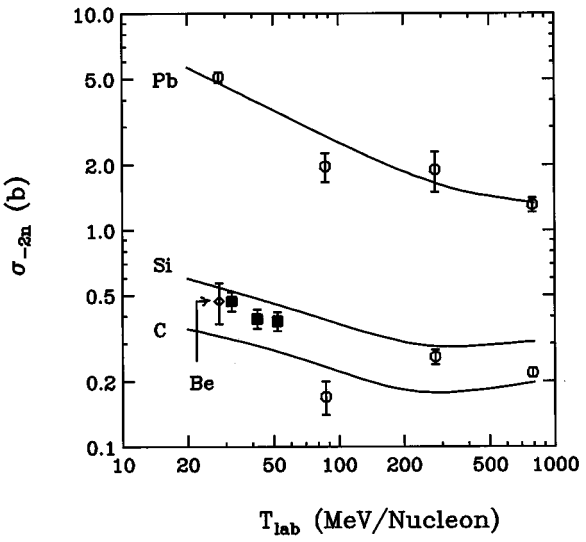

FIG. 9. Measured σ_{-2n} vs energy for ^{11}Li on C, Si, and Pb, compared with microscopic predictions [43]. Present Si data are solid squares; open circles show C and Pb data from [5,21,42,44]. One Be data point [44] is plotted for comparison with the C prediction.

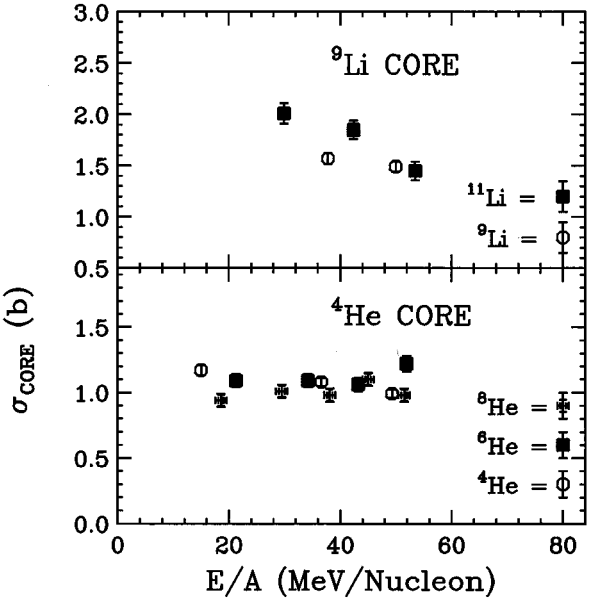

FIG. 10. σ_{CORE} vs energy for ^{9,11}Li data, and for ^{4,6,8}He data; subtraction analysis is described in Sec. IV E of text. The ^{4}He point is taken from [18].

$$\sigma_R(^8\mathrm{He}) - \sigma_{-2n}(^8\mathrm{He}) \neq \sigma_R(^6\mathrm{He}) \tag{9}$$

also holds decisively, as it does at high energy; our ^{6,8}He σ_R's differ by $\approx$0.1 b, while $\sigma_{-2n} \approx 0.4$ b.

V. SUMMARY AND CONCLUSIONS

We have measured σ_R on Si for nine light nuclei including the recognized 2n-halo nuclei ^{6}He and ^{11}Li. Each nucleus was measured at several energies between about 20 and 60A MeV, with an accuracy of about 3%. The magnitudes and energy dependences (except for ^{6}He) of the measurements are all described reasonably well by the optical, strong absorption, and microscopic models, but perhaps best by the last.

Of these nuclei, ^{6}He seems most anomalous in that its lack of energy dependence contradicts all theoretical predictions. Takigawa *et al.* [47] have concluded that Glauber (microscopic) calculations seriously overestimate σ_R for a nucleus with an extended neutron halo. However, the ^{6}He problem is one of the energy dependence of σ_R, not its magnitude, while the microscopic theory gives both correctly for ^{11}Li.

Two-neutron removal was shown to be prolific for the three-halo nuclei. Moreover, $\sigma_{-4n} \approx 0.5\sigma_{-2n}$ was observed for ^{8}He as is also true at 800A MeV. Thus, at our bombarding energies σ_{-2n} has about the same value, 0.4 b, for ^{6}He, ^{8}He, and ^{11}Li, despite their quite different 2n-separation energies: 1.0, 2.1, and 0.3 MeV, respectively. For ^{8}He, having four valence neutrons may compensate for a higher S_{2n}. Curiously, the curvature of the energy dependence does seem correlated with the separation energy (see Fig. 6).

As is true at higher energies, σ_{-2n} is about 20% of σ_R for

^{11}Li. Further, σ_{-2n} is predicted reasonably well by the Esbensen-Bertsch microscopic theory [43] including valence nucleon correlations, even though that theory was intended for use at high energy. In this context we recall that microscopic calculations of σ_R, originally applied [11] to high-energy data, also were found to work very well at low energies [12].

A subtraction analysis [comparison of $\sigma_R - \sigma_{-2n}$ for ^{6}He with $\sigma_R(^4\mathrm{He})$, etc.] like that applied to the high-energy data by Tanihata *et al.* [24] supports the same conclusions as theirs: ^{4}He is a good core within both ^{6}He and ^{8}He, as is ^{9}Li within ^{11}Li.

Our telescope method, now shown to be useful for measuring σ_{-2n}, should measure σ_{-2p} at least as effectively for reactions producing two protons and a fragment with low relative velocities. For example, ^{17}Ne fragmentation must produce at least two protons (the intermediary ^{16}F is unbound) and the products ^{15}O and ^{1}H have ranges in Si of about 4 and 17 mm, compared with 3 mm for ^{17}Ne. Zhukov and Thompson [48] suggest that ^{17}Ne may have a two-proton halo structure. If it does, the fragmentation reaction $^{17}\mathrm{Ne} \rightarrow {}^{15}\mathrm{O} + 2p$ will be prominent and its signature unmistakable.

ACKNOWLEDGMENTS

We thank Professor B. A. Brown, Dr. I. Tanihata, Dr. I. Thompson, and Dr. K. Varga for tabulated matter distributions used in our microscopic calculations; Professor S. M. Austin, Professor P. G. Hansen, and Dr. D. J. Millener for their interest and helpful advice; and Dr. Jack Walton for information about Si(Li) detectors. We also thank the NSCL operations staff for providing excellent beams, and the following undergraduate students for their assistance in setting up and running the experiment: Brendan Field, Ryan McLeod, Linda Nieman, Aaron Seibel, Dan Sisan, Erik Tryggestad, and Jim Young. This work was supported by the National Science Foundation under basic research Grants PHY-9314783 (IUCF), 9402761 (ND), 9214992 (NSCL), 9122067 and 9423659 (Oberlin), 9312428 (UM-Dearborn), and 9208468 and 9512104 (UM-Ann Arbor), and REU Grants PHY-9300011 (ND) and 9424140 (MSU), and by the Department of Energy under Contract W-31-109-ENG-38 to Argonne National Laboratory.

[1] M. C. Mermaz, Phys. Rev. C **50**, 2620 (1994).
[2] I. Tanihata, T. Kobayashi, O. Yamakawa, S. Shimoura, K. Ekuni, K. Sugimoto, N. Takahashi, T. Shimoda, and H. Sato, Phys. Lett. B **206**, 592 (1988), and references therein.
[3] P. G. Hansen and B. Jonson, Europhys. Lett. **4**, 409 (1987).
[4] R. E. Warner *et al.*, Phys. Rev. C **52**, R1166 (1995).
[5] T. Kobayashi *et al.*, Phys. Lett. B **232**, 51 (1989).
[6] M. G. Saint-Laurent *et al.*, Z. Phys. A **332**, 457 (1989).
[7] B. Blank *et al.*, Nucl. Phys. **A555**, 408 (1993), and references therein.
[8] R. E. Warner, H. W. Wilschut, W. F. Rulla, and G. N. Felder, Phys. Rev. C **43**, 1313 (1991).
[9] R. Anne *et al.*, Phys. Lett. B **250**, 19 (1990).
[10] P. J. Karol, Phys. Rev. C **11**, 1203 (1975).
[11] G. F. Bertsch, B. A. Brown, and H. Sagawa, Phys. Rev. C **39**, 1154 (1989).
[12] R. E. Warner and G. N. Felder, Phys. Rev. C **42**, 2252 (1990).
[13] B. M. Sherrill, D. J. Morrissey, J. A. Nolen, Jr., N. Orr, and J. A. Winger, Nucl. Instrum. Methods Phys. Res. Sect. B **70**, 298 (1992).
[14] H. Geissel, T. Schwab, P. Armbruster, J. P. Dufour, E. Hanelt, K.-H. Schmidt, B. Sherrill, and G. Münzenberg, Nucl. Instrum. Methods A **282**, 247 (1989).
[15] W.-Q. Shen, B. Wang, J. Feng, W.-L. Zhan, Y.-T. Zhu, and E.-P. Feng, Nucl. Phys. **A491**, 130 (1989).
[16] Computer code TRIM, version 91.14, J. P. Biersack and J. F. Ziegler (1992). See also J. F. Ziegler, J. P. Biersack, and U. Littmark, *The Stopping and Range of Ions in Solids* (Pergamon, New York, 1985).
[17] C. F. Williamson, J.-P. Boujot, and J. Picard, Commissariat d'Energie Atomique Report No. R3042, 1966.
[18] R. E. Warner, A. M. van den Berg, K. M. Berland, J. D. Hinnefeld, Z. Zhang, Y. T. Zhu, X. Q. Hu, and S. Li, Phys. Rev. C **40**, 2473 (1989).
[19] A. Auce, R. F. Carlson, A. J. Cox, A. Ingemarsson, R. Johansson, P. U. Renberg, O. Sundberg, G. Tibell, and R. Zorro, Phys. Rev. C **50**, 871 (1994).
[20] A. C. C. Villari *et al.*, Phys. Lett. B **268**, 345 (1991).
[21] B. Blank *et al.*, Z. Phys. A **340**, 41 (1991).
[22] T. Kobayashi, O. Yamakawa, K. Omata, K. Sugimoto, T. Shimoda, N. Takahashi, and I. Tanihata, Phys. Rev. Lett. **60**, 2599 (1988).
[23] D. Sackett *et al.*, Phys. Rev. C **48**, 118 (1993).
[24] I. Tanihata, D. Hirata, T. Kobayashi, S. Shimoura, K. Sugimoto, and H. Toki, Phys. Lett. B **289**, 261 (1992).
[25] D. J. Millener (private communication).
[26] G. R. Satchler, Nucl. Phys. **70**, 177 (1965).
[27] H. Rebel, G. W. Schweimer, J. Specht, G. Schatz, R. Löhken, D. Habs, G. Hauser, and H. Klewe-Nebenius, Nucl. Phys. **A182**, 145 (1972).
[28] B. Tatischeff and I. Brissaud, Nucl. Phys. **A155**, 89 (1970).
[29] A. Nadasen, M. McMaster, M. Fingal, J. Tavormina, P. Schwandt, J. S. Winfield, M. F. Mohar, F. D. Becchetti, J. W. Jänecke, and R. E. Warner, Phys. Rev. C **39**, 536 (1989).
[30] A. Nadasen *et al.*, Phys. Rev. C **52**, 1894 (1995).
[31] A. Nadasen and P. G. Roos, Bull Am. Phys. Soc. **29**, 1040 (1984).
[32] S. Kox *et al.*, Phys. Rev. C **35**, 1678 (1987).
[33] S. K. Charagi and S. K. Gupta, Phys. Rev. C **41**, 1610 (1990).
[34] C. W. de Jager, H. de Vries, and C. de Vries, At. Data Nucl. Data Tables **14**, 479 (1974).
[35] K. Varga, Y. Suzuki, and I. Tanihata, Phys. Rev. C **52**, 3013 (1995); K. Varga, private communication.
[36] I. Tanihata *et al.*, Phys. Lett. B **287**, 307 (1992); I. Tanihata, private communication.
[37] K. Varga and Y. Suzuki, Phys. Rev. C **50**, 189 (1994).
[38] A. Csótó, Phys. Rev. C **48**, 165 (1993).
[39] B. A. Brown, A. Csótó, and R. Sherr, Nucl. Phys. **A597**, 66

(1996); B. A. Brown (private communication).
[40] J. S. Vaagen, I. J. Thompson, J. M. Bang, M. V. Zhukov, B. V. Danilin, and D. V. Fedorov, Z. Phys. A **349**, 285 (1994); I. J. Thompson (private communication).
[41] S. Shimoura, in *Proceedings of the International Symposium on Structure and Reactions of Unstable Nuclei*, Niigata, Japan 1991, edited by K. Ikeda and Y. Suzuki (World Scientific, Singapore 1991), p. 132.
[42] F. Humbert *et al.*, Phys. Lett. B **347**, 198 (1995).
[43] H. Esbensen and G. F. Bertsch, Phys. Rev. C **46**, 1552 (1992).
[44] K. Riisager *et al.*, Nucl. Phys. **A540**, 365 (1992).
[45] M. V. Zhukov, A. A. Korsheninnikov, and M. H. Smedberg, Phys. Rev. C **50**, R1 (1994).
[46] Y. Ogawa, K. Kabana, and Y. Suzuki, Nucl. Phys. **A543**, 722 (1992).
[47] N. Takigawa, M. Ueda, M. Kuratani, and H. Sagawa, Phys. Lett. B **288**, 244 (1992).
[48] M. V. Zhukov and I. J. Thompson, Phys. Rev. C **52**, 3505 (1995).